Molecular Biology of the Cell
Vol. 19, 5338–5346, December 2008

Sentan: A Novel Specific Component of the Apical Structure of Vertebrate Motile Cilia

Akiharu Kubo,* Akiko Yuba-Kubo,† Sachiko Tsukita,‡ Shoichiro Tsukita,§ and Masayuki Amagai*

*Department of Dermatology, Keio University School of Medicine, Tokyo 160-8582, Japan; †Mitsubishi Kagaku Institute of Life Sciences, Tokyo 194-8511, Japan; ‡Biological Science Laboratory, Graduate School of Frontier Biosciences, Osaka University, Suita, Osaka 565-0871, Japan; and §Department of Cell Biology, Kyoto University Faculty of Medicine, Kyoto 606-8501, Japan

Submitted July 7, 2008; Revised August 11, 2008; Accepted September 24, 2008
Monitoring Editor: Francis A. Barr

Human respiratory and oviductal cilia have specific apical structures characterized by a narrowed distal portion and a ciliary crown. These structures are conserved among vertebrates that have air respiration systems; however, the molecular components of these structures have not been defined, and their functions are unknown. To identify the molecular component(s) of the cilia apical structure, we screened EST libraries to identify gene(s) that are exclusively expressed in ciliated tissues, are transcriptionally up-regulated during in vitro ciliogenesis, and are not expressed in testis (because sperm flagella have no such apical structures). One of the identified gene products, named sentan, was localized to the distal tip region of motile cilia. Using anti-sentan polyclonal antibodies and electron microscopy, sentan was shown to localize exclusively to the bridging structure between the cell membrane and peripheral singlet microtubules, which specifically exists in the narrowed distal portion of cilia. Exogenously expressed sentan showed affinity for the membrane protrusions, and a protein–lipid binding assay revealed that sentan bound to phosphatidylserine. These findings suggest that sentan is the first molecular component of the ciliary tip to bridge the cell membrane and peripheral singlet microtubules, making the distal portion of the cilia narrow and stiff to allow for better airway clearance or ovum transport.

INTRODUCTION

Motile cilia and flagella are membrane-bound, microtubule-containing cell surface projections that are differentiated by their length, movement characteristics, and numbers per cell (Haimo and Rosenbaum, 1981; Mitchell, 2007; Satir and Christensen, 2007). Flagella-containing cells generally have only one or two flagella, which are long motile structures that beat independently and exhibit an undulating motion. Conversely, cilia are generally much more numerous and are shorter motile projections with an oscillating to-and-fro motion. In humans, flagella are observed only in sperm cells, whereas motile cilia are observed on the respiratory epithelium, along the female reproductive tract, and on the ependymal cells lining the ventricles of the brain.

Early studies using electron microscopy showed that the terminal end of mammalian motile cilia is quite distinct from that of sperm flagella (see Figure 6). At the terminal end of mammalian sperm flagella, peripheral doublet microtubules lose the outer B subfibers or separate into two singlet microtubules. Each singlet microtubule approaches the cell membrane, becomes electron dense and terminates successively. Only a few peripheral singlet subfibers continue to the tip of the sperm tail (Woolley and Nickels, 1985; Afzelius *et al.*, 1995; Suzuki and Nagano, 2002). In contrast, the apical structure of mammalian cilia has a distinct fine structure at the termination site of the axonemal microtubules. The outer B subfibers of peripheral doublet microtubules terminate at the distal portion of cilia, and only the singlet A subfibers continue to the tip. The cell membrane and lateral surface of the singlet A subfibers are connected by filamentous structures that Foliguet and Puchelle (1986) called "lateral spokes." The peripheral A subfibers terminate in an electron-dense capping structure, together with a central pair of singlet microtubules. The capping structure is connected with the cell membrane, and claw-like structures called ciliary crowns are elongated at the surface of the ciliary tip. These specialized capping structures and narrowed distal portions have been reported in not only tracheal and oviductal cilia of various mammals but also chicken tracheal cilia and frog palate cilia (Dirksen and Satir, 1972; Kuhn and Engleman, 1978; Dentler and LeCluyse, 1982; Dalen, 1983; LeCluyse and Dentler, 1984; Foliguet and Puchelle, 1986). These evolutionarily conserved apical structures are considered to make the distal portion stiff to provide better propulsion, promote debris clearance from the trachea, and support ovum transport along the oviduct. To date, many ciliogenesis-related genes have been identified via intensive proteomic studies (Ostrowski *et al.*, 2002), comparative genomics studies (Li *et al.*, 2004; Baron *et al.*, 2007), and genome-wide transcriptional analyses of flagellar regeneration or mucociliary differentiation (Stolc *et al.*, 2005; Hayes *et al.*, 2007; Ross *et al.*, 2007). Nevertheless, the molecular components of these specific apical structures have not been identified.

This article was published online ahead of print in *MBC in Press* (http://www.molbiolcell.org/cgi/doi/10.1091/mbc.E08–07–0691) on October 1, 2008.

Address correspondence to: Akiharu Kubo (akiharukubo@gmail.com).

We hypothesize that the specialized tip structural protein(s) of cilia are not expressed in flagellated cells such as sperm. In this study focused on ciliogenesis-related genes that are not regulated in the testis, we isolated the first component of the specific apical structure of vertebrate tracheal and oviductal cilia. Based on its exclusive localization to the distal tip region of cilia, we have named the protein "sentan," which means "tip" in Japanese.

MATERIALS AND METHODS

Digital Differential Display

Digital differential display (http://www.ncbi.nlm.nih.gov/UniGene/ddd.cgi) was performed on the NCBI UniGene website. In all, 17 EST libraries (190,220 ESTs) of multiple-ciliated epithelia-containing tissues originating from lung, uterus, and trachea were compared with 31 libraries (123,804 ESTs) of simple epithelia-containing tissues originating from colon, liver, kidney, stomach, and intestine or with 62 libraries (250,757 ESTs) originating from those same tissues and brain.

Phylogenetic Tree

The amino acid alignment of sentan was constructed using the ClustalW multiple alignment program and the Boxshade program. The UPGMA phylogenetic tree for sentan was constructed using PROTDIST and NEIGHBOR programs contained in the Phylogeny Inference Package (PHYLIP, ver. 3.6a; Felsenstein, 2003). The following amino acid sequences were used: cow, *Bos taurus*: NP_001071606; horse, *Equus caballus*: ENSECAP00000008198; dog, *Canis familiaris*: ENSCAFP00000010240; human, *Homo sapiens*: ENSP00000341442; chimpanzee, *Pan troglodytes*: ENSPTRP00000026032; mouse, *Mus musculus*: ENSMUSP00000062092; rat, *Rattus norvegicus*: NP_001102568; opossum, *Monodelphis domestica*: ENSMODP00000003611; chicken, *Gallus gallus*: ENSGALP00000011789; anole, *Anolis carolinensis*: the amino acid sequence was assembled using the reverse strand of the genomic sequence of the scaffold_315: 1476029-0475890 and 1473763-1473611 from the *A. carolinensis* draft assembly that was available in February 2007 in the BLAT system of the University of California, Santa Cruz (UCSC); and frog, *Xenopus tropicalis*: the *X. tropicalis* amino acid sequence was assembled using the reverse strand of the genomic sequence of the scaffold_369: 439038-438998, 437962-437823, and 431447-431289 from the *X. tropicalis* whole genome shotgun assembly version 4.1 that was available in August 2005 in the BLAT system of UCSC.

Constructs of Mouse Sentan and Adenovirus Preparation

The EST clone IMAGp998J0313722Q, which contains the full-length mouse sentan [amino acid (aa) 1-147] cDNA, was purchased from RZPD (Berlin, Germany). Mouse sentan (aa 2-147) was tagged with hemagglutinin (HA)-peptide at the NH_2-terminus according to a previously described method (Yuba-Kubo *et al.*, 2005). To construct an expression vector for HA-sentan (pCAG-HA-sentan), an NheI site was introduced at the start codon of the sentan cDNA by PCR, and the PCR fragment and an adapter DNA encoding an HA peptide were introduced into pCAGGS-neodelEcoRI (Niwa *et al.*, 1991), provided by Dr. J. Miyazaki (Osaka University). To make an adenovirus for expressing HA-sentan, the HA-sentan cDNA was subcloned into pShuttle-CMV vector (Stratagene, La Jolla, CA). Recombinant adenovirus containing HA-sentan (rAd-HA-sentan) was then generated by incorporating the expression cassette into pAdEasy-1 vector (Stratagene) according to the manufacturer's instructions (Stratagene). A control adenovirus (rAd-Ctrl) with no transgene was also constructed. The recombinant adenovirus was propagated in AD-293 cells according to the manufacturer's instructions (Stratagene).

Animals

C57BL/6J mice and Japanese white rabbits were purchased from Japan Clea (Tokyo, Japan) and Shimizu Laboratory Supplies (Kyoto, Japan), respectively. For the primary culture of mouse tracheal epithelial cells (MTECs) for the immunofluorescence studies of mouse tissues and for the mRNA and protein preparation from mouse tissues, C57BL/6J mice were killed by intraperitoneal injection of pentobarbital sodium (Nembutal; Dainippon Sumitomo Pharma, Tokyo, Japan). All animal protocols were approved by the animal ethics review board of Keio University (Tokyo, Japan) and Kyoto University (Kyoto, Japan) and conformed to National Institutes of Health guidelines.

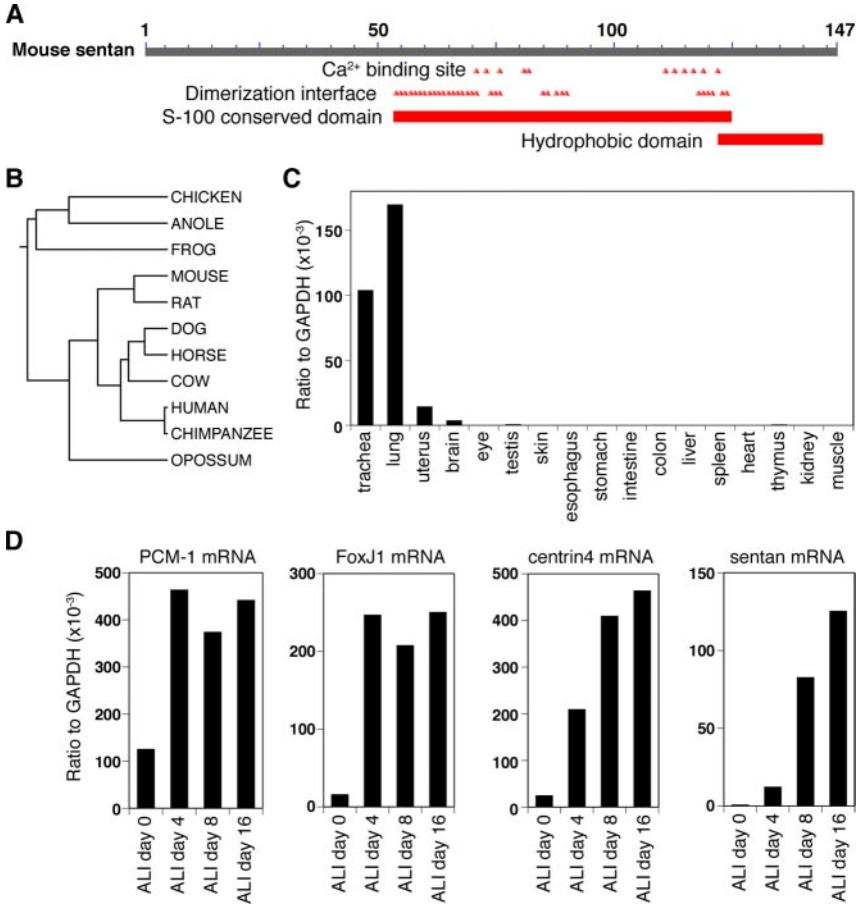

Figure 1. Gene and protein profiles of sentan. (A) Predicted domain structure of mouse sentan protein. (B) Phylogenetic tree of sentan calculated with the program UPGMA, using homologous regions of each species with the corresponding residues of amino acids 49-147 of mouse sentan (Supplemental Figure S1). Sentan is conserved among vertebrates, except fish. (C) Sentan gene expression patterns in various organs from 8-wk-old C57BL/6 mice. Total RNA was prepared from the organs, and SYBR green-based quantitative real-time RT-PCR analysis was performed with specific primers for sentan. The expression of sentan was restricted exclusively to the lung, trachea, and ovary. (D) Gene expression profiles of sentan and other ciliogenesis-related genes (PCM-1, FoxJ1, and centrin4) during in vitro ciliogenesis of cultured primary MTECs. Total RNA was prepared from cultured primary cells before ALI transfer (ALI day 0) and on ALI days 4, 8, and 16. Real-time RT-PCR analysis was performed with specific primers for PCM-1, FoxJ1, centrin4, and sentan. The expression of precursor proteins, PCM-1, and FoxJ1, was induced early in ciliogenesis; however, the expression of a differentiation-specific gene (centrin 4) as well as sentan was induced in the late phase of ciliogenesis. All data were normalized to GAPDH mRNA as an internal control (C and D).

Generation of Polyclonal Antibodies

The cDNA encoding amino acids 1-147 of mouse sentan was subcloned into pGEX 5X-1 (Amersham Pharmacia Biotech, Piscataway, NJ) to produce a fusion protein with glutathione *S*-transferase (GST). The GST fusion protein was expressed in *Escherichia coli*, purified using glutathione Sepharose 4B columns (Amersham Pharmacia Biotech; Smith and Johnson, 1988), and used as an antigen to generate polyclonal antibodies (pAb) in rabbits. Rabbit serum was affinity-purified on a PVDF membrane containing the fusion protein.

Cell Culture and Transfection

Human HeLa cells were cultured in DMEM (Invitrogen-BRL, Rockville, MD) supplemented with 10% fetal calf serum. Human hTERT-RPE-1 retinal pigment epithelial cells were purchased from BD Biosciences Clontech (Palo Alto, CA) and cultured in DMEM/Ham's F12 (Invitrogen-BRL) supplemented with 10% fetal calf serum. Primary cilia were induced by culturing hTERT-RPE-1 cells in medium with 0.25% serum for 48 h. Cultured HeLa and hTERT-RPE-1 cells were transfected with expression vectors by using LipofectAmine2000 (Invitrogen-BRL, Gaithersburg, MD) according to the manufacturer's instructions. C57BL/6J MTECs were harvested from isolated tracheas and grown in primary cultures on support membranes (Transwell Clear; Corning-Costar, Corning, NY) as described previously (You *et al.*, 2002). When the cells were confluent and the transmembrane resistance increased to more than 1000 Ω/cm^2, the medium was removed from the upper chamber to establish an air-liquid interface (ALI). The ciliogenesis induction medium was DMEM/Ham's F12 (1:1) supplemented with 2% NuSerum (Becton-Dickinson, Bedford, MA). For gene transfer to MTECs, the medium was removed from the upper chamber 5 d after initiating the culture (just before ALI day 0). The support membranes were turned upside-down, and rAd-HA-sentan or rAd-Ctrl was delivered for 2 h through the basal surface of the support membrane.

Real-Time PCR

Total RNA was prepared from adult C57BL/6J mouse tissue and cultured MTECs at ALI days 0, 4, 8, and 16 using a RNeasy mini-kit and QIAshredder according to the manufacturer's instructions (QIAGEN, Valencia, CA). The cDNA were reverse-transcribed from total RNA and used as a template for quantitative real-time PCR analysis in duplicate, as described previously (Matsui *et al.*, 2004). Primers were designed to be compatible with a single real-time PCR thermal profile (95°C for 15 min; 40 cycles of 95°C for 15 s, and 60°C for 1 min), such that multiple transcripts could be analyzed simultaneously. All data were normalized to an internal standard [glyceraldehyde-3-phosphate dehydrogenase (GAPDH) mRNA, ΔCt method, User Bulletin 2, Applied Biosystems]. Primer sets were as follows: mouse sentan (NM_177624) forward (5′-AAATGCTTCTGACCCTGATGGTAAAC-3′) and reverse (5′-ATTTTGGCTTGGTTTCTTCTCTCTCTG-3′); mouse PCM-1 (AB029291) forward (5′-TGCCACAGTCAGTAATTCAGAAGAAAC-3′) and reverse (5′-GGGACGGCAGAAACATCACTTATAG-3′); mouse centrin4 (NM_145825) forward (5′-AAAGTTGAACTGAATGACACCCAGAAG-3′) and reverse (5′-GCCCTCATTGCAATCTTTAGTTCTTTC-3′); and mouse GAPDH (NM008084) forward (5′-AAGGTGGTGAAGCAGGCATCTGAG-3′) and reverse (5′-GGAAGAGTGGGAGTTGCTGTTGAAGTC-3′).

Immunoblotting

Trachea and testes were dissected from adult C57BL/6J mice, minced, homogenized in SDS sample buffer (Laemmli, 1970), and boiled for 10 min. HeLa cells were mechanically collected from culture dishes, minced in PBS, homogenized in SDS sample buffer, and boiled for 5 min. Denatured proteins in the boiled samples were separated by SDS-PAGE (5–20% precast gradient gels; Daiichi Kagaku, Tokyo, Japan) and transferred onto Immobilon transfer membranes (Millipore, Bedford, MA). Membranes were then incubated with rabbit anti-sentan pAb or mouse anti-α-tubulin mAb (DM1A; Sigma, St. Louis, MO). Bound antibodies were detected with HRP-conjugated anti-rabbit IgG or HRP-conjugated anti-mouse IgG (Amersham), respectively, and visualized using chemiluminescence (Western Lightning Chemiluminescent Reagent Plus; Perkin Elmer-Cetus, Boston, MA).

Immunofluorescence Microscopy

Fluorescein isothiocyanate (FITC)-conjugated mouse anti-α-tubulin mAb (FITC-DM1A) and mouse anti-acetylated tubulin mAb were purchased from Sigma. Mouse anti-β-tubulin IV mAb, rat anti-HA mAb (3F10), and Texas Red-X-phalloidin were purchased from BioGenex (San Ramon, CA), Roche (Basel, Switzerland), and Molecular Probes (Eugene, OR), respectively. MTECs cultured on Transwell membranes (Corning) were fixed with methanol for 5 min at −20°C, washed in PBS, incubated with 0.12% glycine/PBS for 20 min, and then processed for immunofluorescence microscopy as described previously (Kubo *et al.*, 1999). Mouse tissues were dissected and fixed in 3.7% formaldehyde/PBS for 30 min. Samples were mounted in Tissue-Tek and frozen using liquid nitrogen. Frozen sections, ~12 μm thick, were cut on a cryostat, mounted on poly-L-lysine–coated glass coverslips, air-dried, and soaked in PBS containing 1% Triton X-100 for 10 min. The slides were then rinsed in PBS and processed for immunofluorescence microscopy as described previously (Kubo *et al.*, 1999). HeLa cells and hTERT-RPE-1 cells grown on poly-L-lysine–coated coverslips were fixed with Zamboni's fixative (Stefanini *et al.*, 1967) for 2 h, permeabilized with 0.05% saponin/PBS for 30 min, and then processed for immunofluorescence microscopy as described previously (Kubo *et al.*, 1999). Alexa Fluor 488–conjugated anti-mouse IgG or

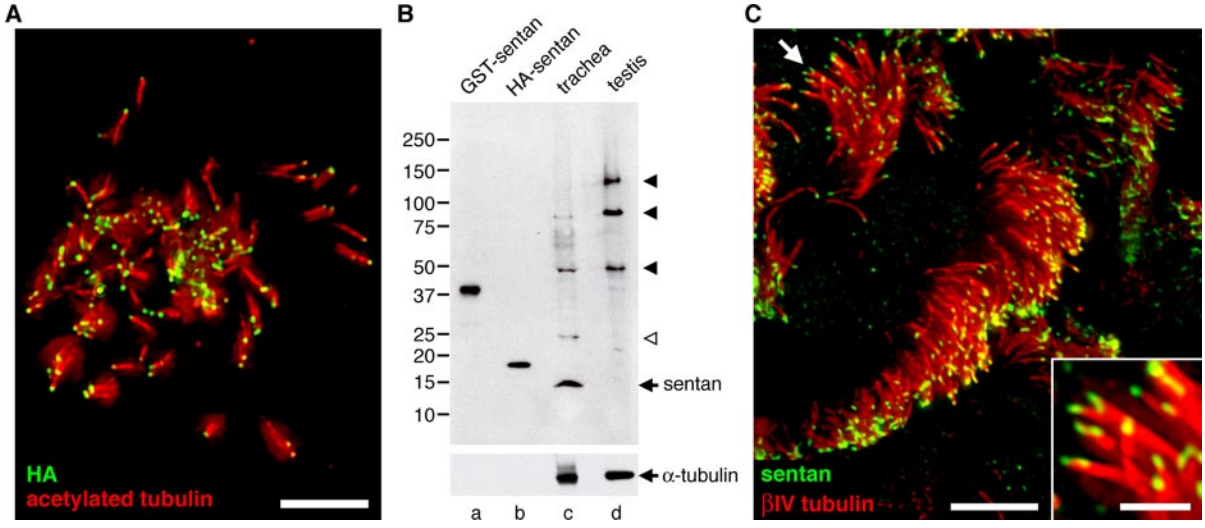

Figure 2. Identification of sentan as a ciliary tip protein. (A) HA-sentan expressed via adenovirus localized to the tip of cilia in cultured primary mouse tracheal cells. Cells were doubly stained with anti-HA rat mAb (green) and anti-acetylated tubulin mouse mAb (red). Bar, 5 μm. (B) Specificity of rabbit anti-sentan pAb. Purified GST fusion protein with full-length mouse sentan was produced in *E. coli* (GST-sentan), total cell lysates of cultured HeLa cells expressing HA-fusion sentan (HA-sentan), and total extracts of mouse trachea (trachea) and testis (testis) were separated by SDS-PAGE, followed by immunoblotting with anti-sentan pAb (top panel) and anti-α-tubulin mAb (bottom panel). The affinity-purified pAb specifically recognized GST-sentan and HA-sentan in lanes a and b, as well as a ~15-kDa band in the tracheal extract (arrow in c), which was not detected in testis extract (d). Equal amounts of protein were loaded in lanes c and d, as confirmed by anti-α-tubulin immunoblotting (bottom panel). The pAb detected some nonspecific bands expressed only in the trachea (open arrowhead), only in the testis, or in both (arrowhead). (C) Endogenous sentan localization to the tip of tracheal cilia. Isolated mouse trachea was doubly stained with anti-sentan pAb (green) and anti-βIV-tubulin mAb (red) and was observed in a whole-mount manner. Indicated area (arrow) is enlarged in the inset. Bars, 10 and 3 μm (inset).

anti-rat IgG and Alexa Fluor 594–conjugated anti-rabbit IgG were purchased from Molecular Probes and used as secondary antibodies. After washing with PBS, the samples were mounted in Mowiol (Calbiochem) and observed under a DeltaVision optical sectioning microscope (Applied Precision Instruments, Issaquah, WA). Whole-cell images were obtained at 0.2-μm intervals in z section, deconvolved, and integrated with DeltaVision software (Applied Precision).

Electron Microscopy

For ultrathin-section electron microscopy, mouse tracheas were fixed in 0.1 M cacodylate buffer containing 0.5% Triton X-100 and 4% paraformaldehyde for 10 min and processed as described previously (Kubo *et al.*, 1999). Goat anti-rabbit IgG coupled to 10-nm gold particles (Nycomed Amersham, Westbury, NY) was used as a secondary antibody. Samples were examined with an electron microscope (JEM 1010; JEOL, Peabody, MA) at an accelerating voltage of 100 kV.

Protein–Lipid Overlay Assay

Protein binding to phospholipids was investigated in a protein–lipid overlay assay using PIP Strips and a membrane lipid array (Echelon Biosciences, Salt Lake City, UT) according to the manufacturer's protocol. In brief, the purified GST-sentan fusion protein was incubated with the membrane for 1 h at room temperature. After intensive washing of the membrane, proteins were detected by incubation with a 1:1000 dilution of anti-GST mouse mAb (GST 3–4C, Zymed, San Francisco, CA), followed by incubation with a 1:10,000 dilution of HRP-conjugated anti-rat IgG (Amersham). Immunoreactive proteins were detected by chemiluminescence (Western Lightning Chemiluminescent Reagent Plus; Perkin Elmer-Cetus).

RESULTS

Identification of Sentan

To identify cilia tip component candidate(s), we first performed digital differential display (http://www.ncbi.nlm.nih.gov/UniGene/ddd.cgi) to compare EST libraries from human multiple-ciliated epithelia-containing tissues and simple epithelia-containing tissues. Trachea, lung, and oviduct-containing uterus were selected for ciliated epithelia-containing tissues. Tissues of the gastrointestinal tract, kidney, and liver, or these tissues plus brain tissue were selected for simple epithelia-containing tissues. As every group includes ESTs derived from primary cilium-bearing epithelial, fibroblastic, mesenchymal, or neuronal cells, we expected motile cilia-specific genes to be isolated. A number of genes were overrepresented in ciliated epithelia-containing tissues (Supplemental Table S1). Among the 96 genes

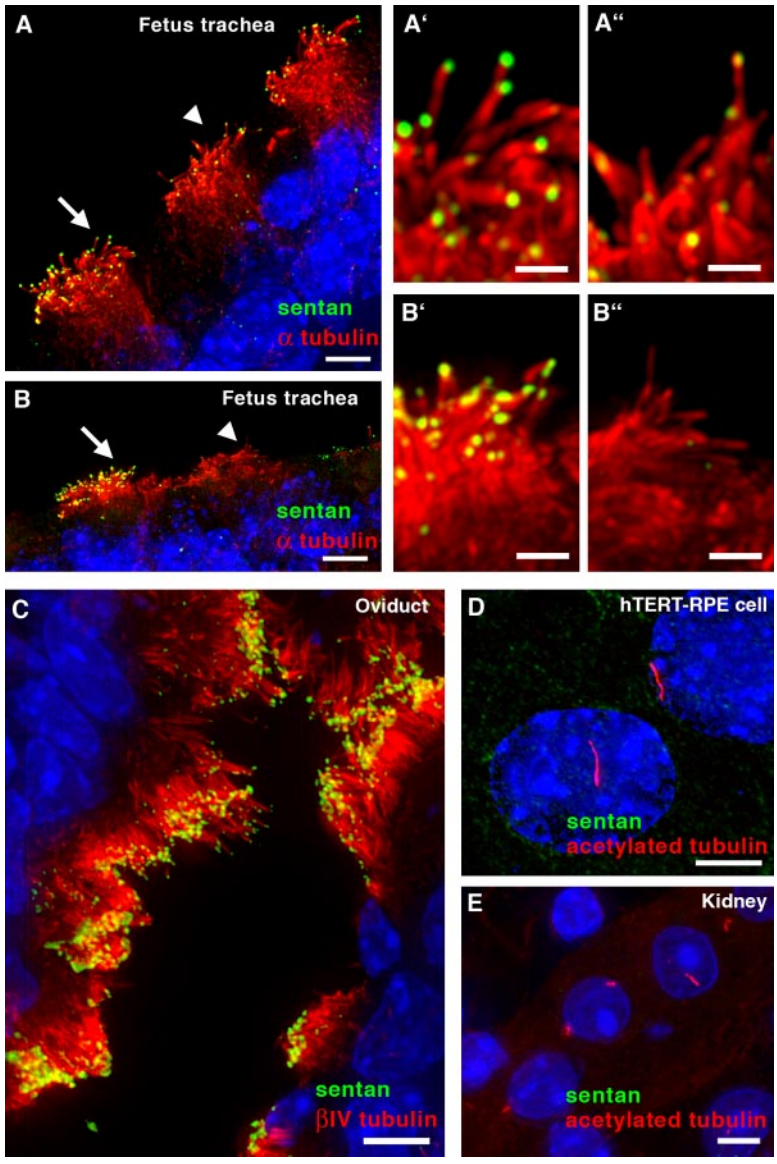

Figure 3. Sentan expression in various types of cilia. (A and B) Sentan localization in the growing cilia of mouse fetal trachea. Vertical sections of trachea were triply stained with anti-sentan pAb (green pseudocolor), FITC-conjugated anti-α-tubulin mAb (red pseudocolor), and DAPI (blue). Each indicated area (arrows and arrowheads) is enlarged: A′, A″, B′, and B″, respectively. Longer cilia had a sentan signal at their tips (arrows in A and B; A′ and B′), shorter ones had only a slight sentan signal (arrowheads in A and A″) or no signal (arrowheads in B and B″). (C) Sentan localization to the tip of oviductal cilia. Oviduct sections were triply stained as described in A. (D and E) No sentan was detected in the tip of primary cilia. Cultured hTERT-RPE1 cells (D) and sections of mouse kidney (E) were triply stained with anti-sentan pAb (green), anti-acetylated tubulin mAb (red), and DAPI (blue). Scale bars, 5 μm (A, B, C, and D), 1 μm (A′, A″, B′, and B″), and 10 μm (E).

identified, those with the highest enrichment were Bardet-Biedl syndrome 1 (BBS1), Tektin1, and EF-hand domain C-terminal containing 1 (EFHC1); these genes have been experimentally identified as cilia-related genes (Larsson *et al.*, 2000; Ikeda *et al.*, 2005; Badano *et al.*, 2006; Marshall, 2008). Next, we examined the tissue expression profiles of these candidates using the EST database. We identified one uncharacterized gene, A430083B19Rik, as being expressed in ciliated epithelia-containing tissues and not in testis tissue, which contained mRNAs of sperm cells whose flagella have no specific tip structures. The protein encoded by A430083B19Rik was a predicted cytoplasmic protein of 147 amino acids with a calculated molecular mass of 16.4 kDa. It comprised conserved S-100–related EF-hand domains (cd00213 of the NCBI conserved domain database) and a hydrophobic domain at its carboxy-terminus (Figure 1A). The genomic database search and phylogenetic analysis revealed that the protein is conserved among tetrapods such as *Xenopus*, anole, chicken, and various mammals, including both eutherians and metatherians, but does not exist in the genomes of fish, invertebrates, or microorganisms (Figure 1B and Supplemental Figure S1). The protein thus appears to be a unique variant of S-100–related protein that is conserved among vertebrates that have air respiration systems. We named the protein "sentan." Quantitative real-time PCR analysis using various mouse tissues confirmed the ciliated-tissue-specific expression of sentan (Figure 1C).

Sentan Is Up-Regulated during Ciliogenesis

Next, we analyzed sentan gene expression during ciliogenesis. Primary MTECs were cultured on a membrane until confluent, and the membrane was transferred to an ALI to induce ciliogenesis. Cultured cells were processed for immunofluorescence studies or harvested for total RNA extraction just before ALI day 0 and on ALI days 4, 8, and 16. On ALI day 0, no cilia were observed at the surface of any cultured cells. The induction of pericentriolar material-1 (PCM-1) protein, a molecular component of fibrous granules that appears in the earliest phases of ciliogenesis (Kubo *et al.*, 1999), was observed in a group of cells within 4 d after ALI transfer. Cilia were observed on ALI day 8, and many mature ciliated cells were observed on ALI day 16 (data not shown). The gene expression of PCM-1 and forkhead box J1 (FoxJ1), an f-box transcription factor essential for ciliogenesis (You *et al.*, 2004), markedly increased on ALI day 4 and was maintained at a high level throughout the ALI culture period (Figure 1D). In contrast, the expression of centrin4, a structural protein of the basal body expressed specifically in ciliated cells (Gavet *et al.*, 2003), gradually increased and exhibited its highest expression level on ALI day 16 (Figure 1D). The expression of sentan was not observed before ALI transfer and was gradually up-regulated during in vitro ciliogenesis, similar to the differentiation-specific gene centrin4 (Figure 1D).

Sentan Is Localized at the Ciliary Tip

We next analyzed the subcellular localization of sentan in ciliated epithelial cells. Full-length cDNA encoding mouse sentan was cloned by PCR using the EST clone IMAGp998J0313722Q as a template. HA-tagged sentan was exogenously expressed in cultured primary MTECs via adenovirus-mediated gene transfer. On day 16, the cultured ALI cells were doubly stained with anti-HA rat mAb and anti-acetylated tubulin mouse mAb (Figure 2A). The acetylated tubulin signal was detected throughout the cilia structure, whereas the HA-tagged sentan signal was concentrated exclusively on the tip of each cilium. We then raised a pAb against recombinant mouse sentan produced in *E. coli*. This pAb recognized a ~15-kDa band in total lysate of mouse trachea but not in the lysate from testis (Figure 2B). The pAb was also immunoreactive with other bands observed in both the trachea and testis. Judging from the calculated molecular mass of mouse sentan (16.4 kDa) and from the reactivity of this pAb with recombinant mouse sentan produced in *E. coli* and with HA-tagged sentan produced in HeLa cells, we concluded that this pAb recognizes mouse sentan.

Next, to examine the subcellular localization of sentan by immunofluorescence microscopy, freshly prepared mouse trachea was immunostained with the anti-sentan pAb and a mAb to βIV-tubulin, a cilia-specific tubulin subtype (Renthal *et al.*, 1993), in a whole-mount manner (Figure 2C). The sentan pAb was immunoreactive with protein found exclusively at the tip of each cilium. Taken together with the cilia tip localization of the exogenously expressed HA-tagged sentan protein, we concluded that this pAb specifically recognizes sentan.

Sentan Is Exclusively Expressed in Ciliated Epithelial Cells

Mouse tracheas from 16-d-old embryos were subjected to immunofluorescence microscopy and showed evidence of ciliogenesis. In the ciliogenetic cells, sentan appeared to localize to the tip of normal- and short-length cilia (Figure 3A). However, sentan did not appear in the very short cilia (Figure 3B), indicating that it localizes to the tip of motile cilia in the growing phase. Next, we investigated sentan localization in other types of cilia. In the multiple-ciliated cells of the oviduct, which have cilia with the same mor-

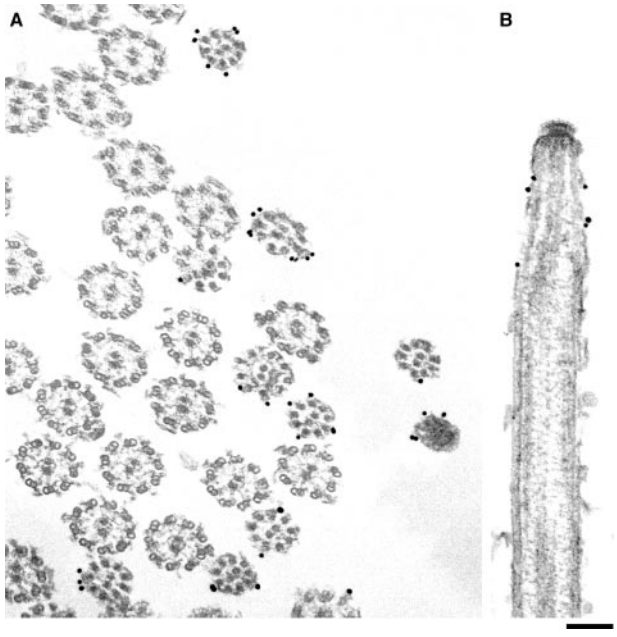

Figure 4. Subcellular localization of sentan at the tip of mouse tracheal cilia. Mouse trachea was treated with 4% paraformaldehyde containing 0.5% Triton X-100 and labeled with anti-sentan pAb. (A) Transverse sections of cilia demonstrating 9 doublets + 2 and 9 singlets + 2 microtubular patterns. Peripheral singlet microtubules were specifically labeled with anti-sentan pAb (10-nm gold particles). Note that peripheral doublet microtubules were not labeled. (B) Longitudinal section of cilia. The outer side of the distal narrowed portion of cilia, the sentan domain, was specifically labeled with anti-sentan pAb. Scale bar, 200 nm.

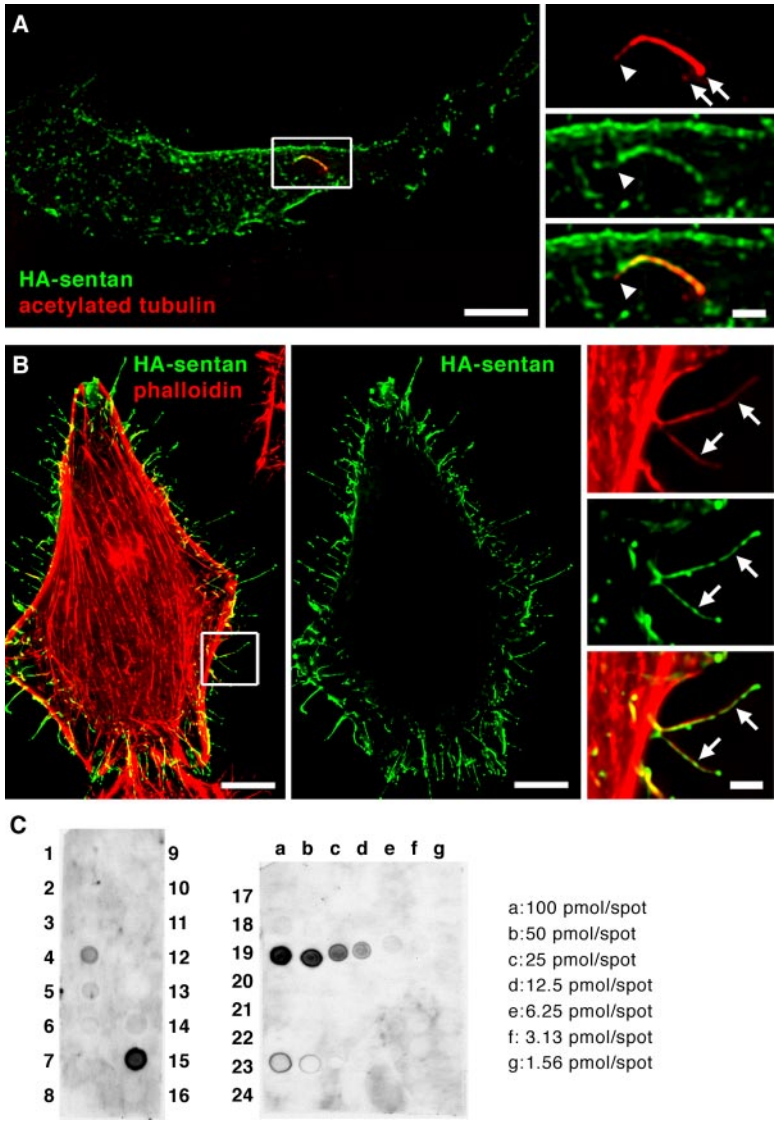

Figure 5. Affinity of sentan for membrane protrusions and phospholipids. (A) Exogenously overexpressed sentan localization in hTERT-RPE cells. Cells were doubly stained with anti-sentan pAb (green) and anti-acetylated tubulin mAb (red). The boxed area is enlarged in the right panels. The acetylated tubulin signal indicated primary cilia and centrioles (arrows). Sentan localized to the peripheral membrane and the primary cilia. A sentan signal was observed in a dotted manner along the axoneme, with some concentration at the apical portion of the cilia. No exclusive localization to the tip was observed (arrowhead). Scale bars, (left) 5 μm and (right) 2 μm. (B) Exogenously overexpressed sentan localization in HeLa cells. Cells were doubly stained with anti-sentan pAb (green) and Texas Red-X-phalloidin (red). The middle panel shows only the sentan signal of the left panel; the boxed area is enlarged in the right panels. Sentan was exclusively localized to the actin-based membrane protrusions (arrows). No sentan signal was detected on the other portions of the cell membrane or actin stress fibers. Scale bars, (left and middle) 5 μm and (right) 2 μm. (C) Phospholipid binding assay of sentan. Biologically active lipids were spotted at 100 pmol per spot in 1–16 and at the indicated amounts in 17–24. Purified GST-sentan was incubated with the PIP-Strip (left) and membrane lipid array (right) and was detected with anti-GST mAb. 1: lysophosphatidic acid; 2: lysophosphocholine; 3: phosphatidylinositol (PtdIns); 4: PtdIns-3-monophosphate (PtdIns(3)P); 5: PtdIns(4)P; 6: PtdIns(5)P; 7: phosphatidylethanolamine; 8: phosphatidylcholine; 9: sphingosine-1-phosphate; 10: PtdIns-3,4-bisphosphate (PtdIns(3,4)P2); 11: PtdIns(3,5)P2; 12: PtdIns(4,5)P2; 13: PtdIns-3,4,5-triphosphate; 14: phosphatidic acid; 15: phosphatidylserine; 16: blank; 17: diacylglycerol; 18: phosphatidic acid; 19: phosphatidylserine; 20: phosphatidylinositol; 21: phosphatidylethanolamine; 22: phosphatidylcholine; 23: phosphatidylglycerol sphingomyelin; and 24: blank.

phology as tracheal cilia, sentan was again observed at the cilial tip (Figure 3C). In contrast, the expression of sentan could not be detected in testis by real-time PCR (Figure 1C), and no specific signal of sentan was detected in the distal portion of sperm flagella (data not shown). To examine the presence or absence of sentan in primary cilia, mouse kidney, and cultured human hTERT-RPE cells were stained with anti-sentan pAb and anti-acetylated tubulin mAb (Figure 3, D and E). No specific sentan signal was detected in primary cilia. These observations indicated that sentan is a component of the specific apical structure of tracheal and oviductal motile cilia.

Sentan Localizes between the Cell Membrane and Peripheral A-Subfibers

We next investigated the subcellular localization of sentan using immunoelectron microscopy. When the apical structure was examined in Triton X-100–treated tracheal epithelial cells by immunoelectron microscopy, anti-sentan pAb was seen to specifically label the membrane side of the singlet peripheral A-tubules, at the distal narrowed portion of the axoneme (Figure 4A). No sentan signal was detected on the A-tubules where they form doublets with B-subfibers. The longitudinal section of the tip showed no sentan label at the electron-dense capping structure. The sentan signal began to be detected on the membrane side of the A-tubules, next to the microtubule plug-in site of the capping structure, in both the transverse and longitudinal sections (Figure 4, A and B).

Affinity of Sentan for the Cell Membrane

These observations indicated that sentan is a component of the bridging structure between the cilia membrane and peripheral singlet microtubules. We next investigated the affinity of sentan for microtubules or the cell membrane. When sentan was exogenously overexpressed in hTERT cells, sentan showed a dotted signal along the axoneme and some concentration to the apical portion of the primary cilia, but no exclusive localization to the tip was observed (Figure 5A). When sentan was overexpressed in HeLa cells, it was localized exclusively to the peripheral membrane protrusions (Figure 5B). Coimmunostaining with actin filaments and microtubules showed that these sentan-localized protrusions were actin-based filopodia

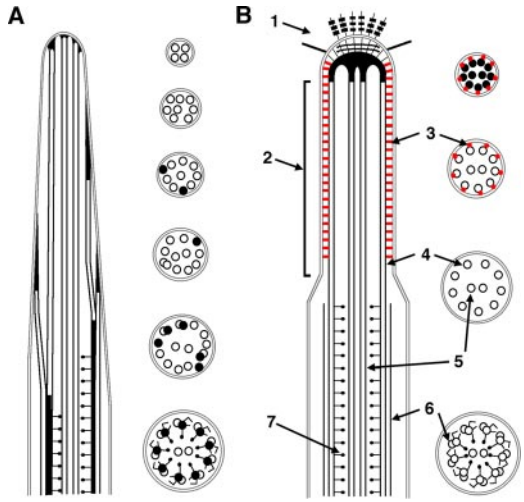

Figure 6. Schematic of the cilia tip structure. Microtubule termination differs between the sperm end piece (A) and the tracheal or oviductal cilia tip (B). Longitudinal sections are represented on the left and transverse sections, on the right (Woolley and Nickels, 1985; modified from Foliguet and Puchelle, 1986). Sentan localized to the A-tubule–membrane linkers is shown in red. 1: ciliary crown and electron-dense capping structure; 2: narrowed distal "sentan domain" of cilia; 3: A-tubule–membrane linkers; 4: peripheral singlet microtubules; 5: central pair of singlet microtubules; 6: B-subfibers of peripheral doublet microtubules; 7: radial spokes.

and did not include microtubules. No sentan colocalization was observed with the actin stress fibers or with microtubules in the cytoplasm (Figure 5B and data not shown).

We next performed a protein–lipid overlay assay to specify the membrane lipid affinity of sentan. GST-fused sentan showed strong binding with phosphatidylserine and very weak binding with phosphatidylinositol-3-monophosphate and phosphatidylglycerol sphingomyelin; GST did not produce any signal in this assay (Figure 5C).

DISCUSSION

Tracheal cilia are thought to play a crucial role in the clearance of mucus and foreign particles from the respiratory tract; disorders of ciliary movement cause immotile cilia syndrome, characterized by chronic sinusitis and bronchiectasis (Ibañez-Tallon *et al.*, 2003; Eley *et al.*, 2005; Zariwala *et al.*, 2007). In patients with immotile cilia syndrome, there is also increased incidence of both female infertility and ectopic pregnancy, because the cilia lining the oviduct normally transport the ovum toward the uterus (Ibañez-Tallon *et al.*, 2003; Eley *et al.*, 2005). Electron micrographs showed that the tips of mammalian tracheal and oviductal cilia have some structural features that are not observed in mammalian sperm flagella or in cilia and flagella of other organisms (Figure 6, A and B). To date, no molecular component of the apical cilial structure has been identified, although a 97-kDa kinetochore antigen was suggested to localize to the microtubule capping structure (Miller *et al.*, 1990).

In this study, we identified sentan as the first molecular component of the apical structure of tracheal and oviductal cilia. Sentan localized exclusively between the ciliary membrane and the peripheral singlet microtubules at the distal narrowed portion of cilia, suggesting that sentan is a molecular component of the linker structure that bridges the ciliary membrane and the peripheral singlet microtubules (Figure 6B; called "lateral spokes" in Foliguet and Puchelle, 1986). According to the genomic database, sentan is found in most mammals, including eutherians and metatherians, and in birds, reptiles, and amphibians. However, the genomic database does not suggest its presence in invertebrates or fish such as *Tetraodon nigroviridis*, *Takifugu rubripes*, *Danio rerio*, and *Oryzias latipes*. Consistent with in silico analyses, a narrowed distal portion has been observed in cilia in the trachea of various mammals, in chickens, in the palate of frogs, and in the ciliated grooves of frogs between the choanae (nasal openings) and the esophageal opening (Kuhn and Engleman, 1978; Dentler and LeCluyse, 1982; LeCluyse and Dentler, 1984; Foliguet and Puchelle, 1986); however, it has not been observed in fish or invertebrates (Dentler, 1980). We speculate that sentan is indispensable for the morphogenesis of the narrowed distal portion of cilia and that sentan and this specific structure appeared early in the evolution of air respiratory systems. These structures are most likely widely conserved among tetrapods because of the need to clear mucus and debris from the airway. We propose naming the sentan-positive distal narrowed portion of cilia the "sentan domain" and the sentan-positive microtubule-membrane bridges "A-tubule–membrane linkers" (Figure 6B).

Early electron microscopy studies of growing cilia of the frog palate showed that a disk-shaped, electron-dense plate forms at the tip of cilia during the first micron of growth; the maturation of the capping structure is complete in cilia longer than 2 μm (Portman *et al.*, 1987). In human cilia, the peripheral singlet microtubules and the sentan domain are observed when cilia are longer than 3 μm (Foliguet and Puchelle, 1986). The formation of the capping structure suggests that only the singlet A-tubules are capped and possibly stabilized, making it reasonable to hypothesize that the sentan domain is formed after the formation of the capping structure. In agreement with this conjecture, sentan begins to localize to the tip only after cilia of the fetal trachea reach ~3 μm in length. These results indicate that the formation of the sentan domain with peripheral singlet microtubules and the recruitment of sentan occur simultaneously.

Overexpressed sentan localized to cell peripheral protrusions in hTERT-RPE cells; however, a dotted signal along the axoneme and some concentration at the apical portion of primary cilia were observed. This dotted pattern suggests that exogenous sentan is transported on intraflagellar transport particles and, as a result, concentrates at the apical portion of cilia (Pazour and Rosenbaum, 2002; Cole, 2005; Sloboda, 2005; Follit *et al.*, 2006; Hou *et al.*, 2007; Omori *et al.*, 2008; Scholey, 2008). The dotted pattern and the fact that only a very small portion of exogenously expressed sentan localized to primary cilia also indicated that sentan is not recruited to the spaces between the cell membrane and peripheral doublet microtubules in primary cilia or in mature or growing tracheal cilia. When sentan was overexpressed in HeLa cells, it clearly localized to actin-related membrane protrusions such as filopodia. As sentan did not colocalize with actin stress fibers and because an immunoprecipitation assay of HA-sentan in HeLa cells failed to detect any cosedimentation proteins, including actin (unpublished data), sentan localization to the membrane protrusion appears to be independent of actin fibers. The strong affinity of sentan for phosphatidylserine, one of the major inner leaflet phospholipids, indicates that sentan may localize to the protrusion by direct binding to the cell membrane.

Why does sentan localize only around the peripheral singlet microtubules and not around the peripheral doublet

microtubules in motile cilia? One hypothesis is that the cell membrane affinity of sentan is dependent on the curvature of the membrane; as a result, sentan localization to the protrusions could be dependent on their diameter. Interestingly, the diameter of the distal portion of cilia is almost equivalent to the diameter of HeLa cell protrusions: 150 and ~120–130 nm, respectively (Fisher and Cooper, 1967; Porter *et al.*, 1974; Foliguet and Puchelle, 1986; Hosaka *et al.*, 1993). These diameters are smaller than that of cilia axoneme (~250–300 nm) and larger than that of microvilli (~80 nm) present on the apical surface of tracheal epithelial cells (Simionescu and Simionescu, 1976; Dalen, 1983); neither of these recruited adenovirus-overexpressed or native sentan, which supports the idea that sentan localization is dependent on the curvature of the membrane. Another hypothesis is that sentan localization is dependent on specifically modified tubulin found in peripheral singlet microtubules. Axonemal tubulin has been reported to harbor multiple posttranslational modifications (e.g., polyglutamylation by tubulin tyrosine ligase-like proteins or monomeric or polymeric glycylation by unknown enzymes; Redeker *et al.*, 1994; Million *et al.*, 1999; Ikegami *et al.*, 2006; Pathak *et al.*, 2007), and ciliary tip tubulin has been shown to be excluded from monomeric glycylation (Dossou *et al.*, 2007). It is possible that specifically modified singlet peripheral microtubules recruit sentan via direct binding or via binding with specific microtubule-binding proteins. The elucidation of other components associated with singlet microtubules in the sentan domain of cilia could provide an understanding of the interplay between sentan and singlet peripheral microtubules.

In conclusion, we identified sentan as the first molecular component of the apical structure of vertebrate tracheal and oviductal cilia. Sentan is also the first protein to be identified as linking ciliary microtubules to the ciliary membrane in mammalian tissue. The identification of sentan provides valuable information regarding the molecular structure of the characteristic sentan domain of vertebrate motile cilia and is an important step in understanding the contribution of the sentan domain to cilia function. Further detailed analysis of the sentan domain of cilia and the sentan molecule should help elucidate the molecular mechanism of ciliogenesis and the evolution of air respiration systems.

ACKNOWLEDGMENTS

We thank all of the members of our laboratories (Department of Cell Biology, Faculty of Medicine, Kyoto University and Department of Dermatology, Keio University School of Medicine) for helpful discussions. We also thank Hiromi Doi for her excellent technical assistance. This manuscript is dedicated to the memory of Professor Shoichiro Tsukita. This work was supported in part by a Grant-in-Aid for Young Scientists (B) to A.K. from the Ministry of Education, Culture, Sports, Science, and Technology of Japan and Keio University Research Grants for Life Science and Medicine to A.K. from the Keio University Medical Science Fund.

REFERENCES

Afzelius, B. A., Dallai, R., Lanzavecchia, S., and Bellon, P. L. (1995). Flagellar structure in normal human spermatozoa and in spermatozoa that lack dynein arms. Tiss. Cell *27*, 241–247.

Badano, J. L., Mitsuma, N., Beales, P. L., and Katsanis, N. (2006). The ciliopathies: an emerging class of human genetic disorders. Annu. Rev. Genomics Hum. Genet. *7*, 125–148.

Baron, D. M., Ralston, K. S., Kabututu, Z. P., and Hill, K. L. (2007). Functional genomics in *Trypanosoma brucei* identifies evolutionarily conserved components of motile flagella. J. Cell Sci. *120*, 478–491.

Cole, D. G. (2005). Intraflagellar transport: keeping the motors coordinated. Curr. Biol. *15*, R798–R801.

Dalen, H. (1983). An ultrastructural study of the tracheal epithelium of the guinea-pig with special reference to the ciliary structure. J. Anat. *136*, 47–67.

Dentler, W. L. (1980). Structures linking the tips of ciliary and flagellar microtubules to the membrane. J. Cell Sci. *42*, 207–220.

Dentler, W. L., and LeCluyse, E. L. (1982). Microtubule capping structures at the tips of tracheal cilia: evidence for their firm attachment during ciliary bend formation and the restriction of microtubule sliding. Cell Motil. *2*, 549–572.

Dirksen, E. R., and Satir, P. (1972). Ciliary activity in the mouse oviduct as studied by transmission and scanning electron microscopy. Tiss. Cell *4*, 389–403.

Dossou, S. J., Bré, M. H. and Hallworth, R. (2007). Mammalian cilia function is independent of the polymeric state of tubulin glycylation. Cell Motil. Cytoskelet. *64*, 847–855.

Eley, L., Yates, L. M., and Goodship, J. A. (2005). Cilia and disease. Curr. Opin. Genet. Dev. *15*, 308–314.

Felsenstein, J. (2003). PHYLIP (Phylogeny Inference Package), version 3.6a. Distributed by the author. Department of Genetics, University of Washington, Seattle.

Fisher, H. W., and Cooper, T. W. (1967). Electron microscope studies of the microvilli of HeLa cells. J. Cell Biol. *34*, 569–576.

Foliguet, B., and Puchelle, E. (1986). Apical structure of human respiratory cilia. Bull. Eur. Physiopathol. Respir. *22*, 43–47.

Follit, J. A., Tuft, R. A., Fogarty, K. E., and Pazour, G. J. (2006). The intraflagellar transport protein IFT20 is associated with the Golgi complex and is required for cilia assembly. Mol. Biol. Cell *17*, 3781–3792.

Gavet, O., Alvarez, C., Gaspar, P., and Bornens, M. (2003). Centrin4p, a novel mammalian centrin specifically expressed in ciliated cells. Mol. Biol. Cell *14*, 1818–1834.

Haimo, L. T., and Rosenbaum, J. L. (1981). Cilia, flagella, and microtubules. J. Cell Biol. *91*, 125s–130s.

Hayes, J. M., Kim, S. K., Abitua, P. B., Park, T. J., Herrington, E. R., Kitayama, A., Grow, M. W., Ueno, N., and Wallingford, J. B. (2007). Identification of novel ciliogenesis factors using a new in vivo model for mucociliary epithelial development. Dev. Biol. *312*, 115–130.

Hosaka, S., Usuda, N., and Nagata, T. (1993). An ultrastructural study on HeLa cells cultured in roller bottles forming aggregates. Med. Electron Microsc. *26*, 125–131.

Hou, Y., Qin, H., Follit, J. A., Pazour, G. J., Rosenbaum, J. L., and Witman, G. B. (2007). Functional analysis of an individual IFT protein: IFT46 is required for transport of outer dynein arms into flagella. J. Cell Biol. *176*, 653–665.

Ibañez-Tallon, I., Heintz, N., and Omran, H. (2003). To beat or not to beat: roles of cilia in development and disease. Hum. Mol. Genet. *12*, R27–R35.

Ikeda, T., Ikeda, K., Enomoto, M., Park, M. K., Hirono, M., and Kamiya, R. (2005). The mouse ortholog of EFHC1 implicated in juvenile myoclonic epilepsy is an axonemal protein widely conserved among organisms with motile cilia and flagella. FEBS Lett. *579*, 819–822.

Ikegami, K., Mukai, M., Tsuchida, J., Heier, R. L., Macgregor, G. R., and Setou, M. (2006). TTLL7 is a mammalian beta-tubulin polyglutamylase required for growth of MAP2-positive neurites. J. Biol. Chem. *281*, 30707–30716.

Kubo, A., Sasaki, H., Yuba-Kubo, A., Tsukita, S., and Shiina, N. (1999). Centriolar satellites: molecular characterization, ATP-dependent movement toward centrioles and possible involvement in ciliogenesis. J. Cell Biol. *147*, 969–980.

Kuhn, C., and Engleman, W. (1978). The structure of the tips of mammalian respiratory cilia. Cell Tiss. Res. *186*, 491–498.

Laemmli, U. K. (1970). Cleavage of structural proteins during the assembly of the head of bacteriophage T4. Nature *227*, 680–685.

Larsson, M., Norrander, J., Gräslund, S., Brundell, E., Linck, R., Ståhl, S., and Höög, C. (2000). The spatial and temporal expression of Tekt1, a mouse tektin C homologue, during spermatogenesis suggest that it is involved in the development of the sperm tail basal body and axoneme. Eur. J. Cell Biol. *79*, 718–725.

LeCluyse, E. L., and Dentler, W. L. (1984). Asymmetrical microtubule capping structures in frog palate cilia. J. Ultrastruct. Res. *86*, 75–85.

Li, J. B. *et al.* (2004). Comparative genomics identifies a flagellar and basal body proteome that includes the BBS5 human disease gene. Cell *117*, 541–552.

Marshall, W. F. (2008). The cell biological basis of ciliary disease. J. Cell Biol. *180*, 17–21.

Matsui, T. *et al.* (2004). Identification of novel keratinocyte-secreted peptides dermokine-alpha/-beta and a new stratified epithelium-secreted protein gene complex on human chromosome 19q13.1. Genomics *84*, 384–397.

Miller, J. M., Wang, W., Balczon, R., and Dentler, W. L. (1990). Ciliary microtubule capping structures contain a mammalian kinetochore antigen. J. Cell Biol. *110*, 703–714.

Million, K., Larcher, J., Laoukili, J., Bourguignon, D., Marano, F., and Tournier, F. (1999). Polyglutamylation and polyglycylation of alpha- and beta-tubulins during in vitro ciliated cell differentiation of human respiratory epithelial cells. J. Cell Sci. *112*, 4357–4366.

Mitchell, D. R. (2007). The evolution of eukaryotic cilia and flagella as motile and sensory organelles. Adv. Exp. Med. Biol. *607*, 130–140.

Niwa, H., Yamamura, K., and Miyazaki, J. (1991). Efficient selection for high-expression transfectants with a novel eukaryotic vector. Gene *108*, 193–199.

Omori, Y., Zhao, C., Saras, A., Mukhopadhyay, S., Kim, W., Furukawa, T., Sengupta, P., Veraksa, A., and Malicki, J. (2008). Elipsa is an early determinant of ciliogenesis that links the IFT particle to membrane-associated small GTPase Rab8. Nat. Cell Biol. *10*, 437–444.

Ostrowski, L. E., Blackburn, K., Radde, K. M., Moyer, M. B., Schlatzer, D. M., Moseley, A., and Boucher, R. C. (2002). A proteomic analysis of human cilia: identification of novel components. Mol. Cell Proteomics *1*, 451–465.

Pathak, N., Obara, T., Mangos, S., Liu, Y., and Drummond, I. A. (2007). The zebrafish fleer gene encodes an essential regulator of cilia tubulin polyglutamylation. Mol. Biol. Cell *18*, 4353–4364.

Pazour, G. J., and Rosenbaum, J. L. (2002). Intraflagellar transport and cilia-dependent diseases. Trends Cell Biol. *12*, 551–555.

Porter, K. R., Fonte, V., and Weiss, G. (1974). A scanning microscope study of the topography of HeLa cells. Cancer Res. *34*, 1385–1394.

Portman, R. W., LeCluyse, E. L., and Dentler, W. L. (1987). Development of microtubule capping structures in ciliated epithelial cells. J. Cell Sci. *87*, 85–94.

Redeker, V., Levilliers, N., Schmitter, J. M., Le Caer, J. P., Rossier, J., Adoutte, A., and Bré, M.H. (1994). Polyglycylation of tubulin: a posttranslational modification in axonemal microtubules. Science *266*, 1688–1691.

Renthal, R., Schneider, B. G., Miller, M. M., and Ludueña, R. F. (1993). Beta IV is the major beta-tubulin isotype in bovine cilia. Cell Motil. Cytoskelet. *25*, 19–29.

Ross, A. J., Dailey, L. A., Brighton, L. E., and Devlin, R. B. (2007). Transcriptional profiling of mucociliary differentiation in human airway epithelial cells. Am. J. Respir. Cell. Mol. Biol. *37*, 169–185.

Satir, P., and Christensen, S. T. (2007). Overview of structure and function of mammalian cilia. Annu. Rev. Physiol. *69*, 377–400.

Scholey, J. M. (2008). Intraflagellar transport motors in cilia: moving along the cell's antenna. J. Cell Biol. *180*, 23–29.

Simionescu, N., and Simionescu, M. (1976). Galloylglucoses of low molecular weight as mordant in electron microscopy. I. Procedure, and evidence for mordanting effect. J. Cell Biol. *70*, 608–621.

Sloboda, R. D. (2005). Intraflagellar transport and the flagellar tip complex. J. Cell Biochem. *94*, 266–272.

Smith, D. B., and Johnson, K. S. (1988). Single-step purification of polypeptides expressed in *Escherichia coli* as fusions with glutathione S-transferase. Gene *67*, 31–40.

Stefanini, M., De Martino, C., and Zamboni, L. (1967). Fixation of ejaculated spermatozoa for electron microscopy. Nature *216*, 173–174.

Stolc, V., Samanta, M. P., Tongprasit, W., and Marshall, W. F. (2005). Genome-wide transcriptional analysis of flagellar regeneration in *Chlamydomonas reinhardtii* identifies orthologs of ciliary disease genes. Proc. Natl. Acad. Sci. USA *102*, 3703–3707.

Suzuki, F., and Nagano, T. (2002). Morphological relationship between the plasma membrane and the microtubules in the end piece of the boar spermatozoon. J. Electron Microsc. *29*, 190–192.

Woolley, D. M., and Nickels, S. N. (1985). Microtubule termination patterns in mammalian sperm flagella. J. Ultrastruct. Res. *90*, 221–234.

You, Y., Richer, E. J., Huang, T., and Brody, S. L. (2002). Growth and differentiation of mouse tracheal epithelial cells: selection of a proliferative population. Am. J. Physiol. Lung Cell Mol. Physiol. *283*, L1315–L1321.

You, Y., Huang, T., Richer, E. J., Schmidt, J. E., Zabner, J., Borok, Z., and Brody, S. L. (2004). Role of f-box factor foxj1 in differentiation of ciliated airway epithelial cells. Am. J. Physiol. Lung Cell Mol. Physiol. *286*, L650–L657.

Yuba-Kubo, A., Kubo, A., Hata, M., and Tsukita, S. (2005). Gene knockout analysis of two gamma-tubulin isoforms in mice. Dev. Biol. *282*, 361–373.

Zariwala, M. A., Knowles, M. R., and Omran, H. (2007). Genetic defects in ciliary structure and function. Annu. Rev. Physiol. *69*, 423–450.